Elastic scattering of traveling phonons by discrete breathers as a time-periodic scatterer in the one-dimensional discrete nonlinear Schrödinger model: Exact analysis

Priyadarshi Majumdar*
Jyotinagar Bidyasree Niketan H.S. School, 41 Jyotinagar, Kolkata 700 108, India

Subhendu Panda
JM 12/1 Aswaninagar, Baguiati, Kolkata 700 059, India

(Received 10 October 2009; revised manuscript received 15 August 2010; published 27 September 2010)

Discrete nonlinear Schrödinger model is a nonlinear lattice model used to investigate different nonlinear phenomena arising in many physical contexts. In this work we used this model to observe linear traveling phonon scattering by time-periodic discrete breathers in the *piecewise smooth* (PWS) version of nonlinearity. In one-dimensional system the single-channel scattering is found to be elastic (with the incoming and outgoing fluxes of energy being equal to each other). Considering one-site symmetric breather solution we are able to calculate the exact expression for the transmission coefficient (T) or the ratio of the transmitted to incident flux of energy in such a system using *transfer-matrix* formalism. From the condition of perfect transmission ($T=1$, and hence reflection coefficient $R=0$) or the ratio of reflected to incident flux of energy for elastic scattering is zero, our observation shows that perfect transmission happens to appear at the threshold of a localized mode, which occurs at the band edge of the extended eigenmodes (plane waves). We have also presented the results obtained from the condition of perfect reflection. The advantage of using the PWS version of nonlinearity in the model is that all the results derived are exact. Numerical simulations complement our results.

DOI: 10.1103/PhysRevE.82.036607 PACS number(s): 05.45.Yv, 42.65.Tg

I. INTRODUCTION

There is a growing interest in the literature of nonlinear physics concerning modeling and analysis of different lattices that can be taken as prototypical systems. Investigations reveal that the existing laws of linear physics cannot properly describe many physical phenomena. One such important observation was the discovery of localized solutions known as *discrete breathers* (DBs).

Discrete breathers, by definition, are time-periodic and spatially localized excitations observed frequently in discrete nonlinear Hamiltonian systems. After their discovery many observations have been made both in the theoretical and numerical fields [1–8] related to their existence, stability, and other important properties. One such observation, in particular, related to their existence and stability reveals that the presence of nonlinearity and discreteness are two essential conditions for the generic existence of these localized objects. These conditions also make them distinct from other types of localized modes (LMs), e.g., Anderson modes [9]. Breathers are observed in translationally invariant systems (e.g., perfectly regular lattice) induced by nonlinearity (as we discretize a partial differential equation to its corresponding differential-difference form it loses the continuous translational symmetry, but it still possesses discrete translational symmetry), but for Anderson modes we have to break the translational invariance or homogeneity by introducing disorder or impurity to observe the localized objects.

Linear stability of DBs only states that the solutions are stable against small perturbations. This implies in turn that any small perturbation applied to a DB does not grow exponentially with time. Numerical investigations reveal that many physical situations can be satisfactorily explained by considering the interactions between various DBs and also their interactions with the environment. Therefore, to study these interactions their responses in any experiment are important to a great extent. In this context we are interested here in one particular type of such interactions that involves *elastic scattering* of phonons by a DB acting as a scattering center. Moreover, the study of the dynamical properties of different nonlinear lattices also reveals that the existence of the LM threshold in the linearized problem about the DB solutions provides a systematic way to explore some important aspects of DBs, e.g., quasiperiodicity, pinning mode, and mobility of the solution. Our analysis of phonon scattering by DB exhibits that the existence of creation threshold for the LM is responsible for PT in the process. Numerical investigations show that some of the *Floquet modes* [10] are localized about the DB solutions. These can be taken as LMs about the localized solutions [11]. In our analyses we will show that the presence of those internal modes is responsible for the occurrences of *perfect transmission* (PT) and *perfect reflection* (PR). In [11] the author showed similar phenomena by considering elastic scattering of phonons by a static kink used as a scatterer in the discrete nonlinear Schrödinger (DNLS) model. But we present our results based on the scattering of phonons by DBs, which are time-periodic and spatially localized solutions. Observations show that the scattering phenomenon changes drastically at the threshold of these *localized modes*. In our analysis, we investigate the phonon scattering by DBs by studying the transmission and the reflection coefficients. Important results are that we are able to find exact analytical expression for the transmission coeffi-

*majumdar_priyadarshi@yahoo.com

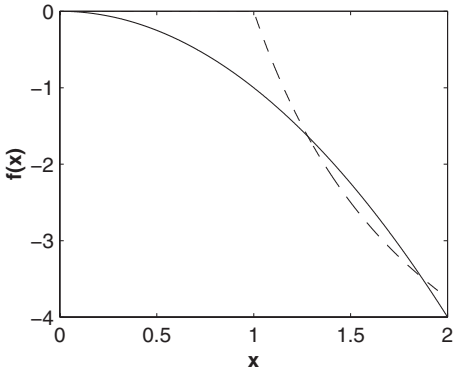

FIG. 1. Comparison between the functional natures: $f(x)=-\gamma|x|^2$ for $\gamma=1$, the conventional form (solid line), and the PWS version $f(x)=\gamma(1-1/|x|)\Theta(|x|-1)$ for a properly scaled value of γ (=7.5) (dashed line) show an overlapping region confirming our assumption.

cient for this scattering process and show that PT and PR are connected with the *internal modes* of the DBs [12]. The method can further be developed by taking corrections to this linear process due to nonlinearity to its lowest significant order.

In this paper we mainly investigate the elastic scattering of traveling phonons by time-periodic DBs in the piecewise smooth (PWS) version of the DNLS model. The important feature is that although our scattering center is a time-periodic and spatially localized object, the nature of scattering related to PT and PR admits the results obtained in [11]. Another distinguishing feature of our work is that all the results are exact, which are again complemented by the numerical simulation (using MATLAB in Intel platform). We apply transfer-matrix formalism [13,14] to calculate the transmission and the reflection coefficients in this model. This work is an extension of earlier works [15,16] where exact analytical results related to the construction and linear stability of the discrete breathers and an expression for the threshold value of localized modes at the band edge in the PWS version of the DNLS model have been derived. We have also done similar works in the PWS version of the *nonlinear discrete Klein-Gordon* (NDKG) model in another paper [17].

The PWS version of nonlinearity can find its usefulness even in those physical contexts where the conventional cubic type of nonlinearities is applicable. Some of those areas are Raman scattering spectra of complex electronic materials [18–20], manifestation of an abrupt and irreversible delocalization of Bose-Einstein condensates trapped in two-dimensional (2D) optical lattices [21,22], instability of localized modes in coupled arrays of optical lattices [23,24], etc. where cubic model has already been analyzed. These results are mostly based on the computer simulation and are verified by the laboratory experiments. These are not solvable by any easy analytical means. The advantage of the PWS model over the cubic model is that we can obtain all those results analytically exact, which may not be possible for the latter. Comparing PWS type [Eq. (9)] and the conventional cubic type of nonlinearities $xf(x)$ [where $f(x)=-\gamma|x|^2$; see Fig. 1], we find that for a definite set of values of parameters the nature of both functions is very close to each other in a certain region (in between 1 and 2) for two different γ values (nonlinearity parameter) for each of the PWS model and the conventional cubic model. In this region therefore, our analytical results must qualitatively agree with the results of the DNLS model with cubic type of nonlinearity. Hence, the physical contexts where the DNLS equation with cubic type of nonlinearity raised can be the area where the PWS type of nonlinearity is equally applicable.

The present paper is organized as follows. In Sec. II we briefly discuss the transfer-matrix formalism and its connection with the phonon-breather scattering. Section III discusses some earlier works on one-site monochromatic discrete breathers and their stability. In Sec. IV we present exact scattering analysis in the PWS version of the DNLS model supported by numerical simulations. Finally Sec. V ends with our conclusion and scope for further work.

II. TRANSFER-MATRIX FORMALISM

Our analysis of phonon scattering by DBs is based on transfer-matrix formalism mentioned earlier. This formalism is quite a convenient mathematical tool to derive the transmission and reflection coefficients. We present in this section the main features of this method that are related to our analysis.

Accordingly, with the help of a matrix arising from a dynamical equation, we can find a relation between the amplitudes of the incoming and the outgoing waves. That particular matrix is known as the transfer matrix and is central to the entire formalism. To elaborate it we consider the DNLS equation defined on a lattice model as

$$i\dot{\psi}_n + V(\psi_{n+1} + \psi_{n-1}) + f(|\psi_n|)\psi_n = 0 \quad (n = 0, \pm 1, \pm 2, \ldots). \tag{1}$$

The modulus of the complex wave function $\psi_n(t)$ and V stand for the oscillation amplitude at the nth lattice point and the nearest-neighbor coupling parameter between the lattice sites, respectively. The last term in Eq. (1) represents the nonlinear function in the proposed lattice model. The DB solution admitted by the model is

$$\psi_n(t) = \phi_n e^{-i\omega t}, \tag{2}$$

where ϕ_n and ω are the breather amplitude at the nth site (which is real and independent of time) and the breather frequency, respectively.

In the scattering process, phonons are simply the solutions of the linearized time-evolution equation for small-amplitude perturbation $u_n(t)$ applied to the breather solution. With the perturbed solution $[\psi_n(t)+u_n(t)]$ the evolution equation for $u_n(t)$ [as obtained from Eq. (1)] looks like

$$i\dot{u}_n + V(u_{n+1} + u_{n-1}) + g = 0, \tag{3}$$

where g is the linearized version of the nonlinear function [represented by the last term in Eq. (1)] obtained after the application of perturbation and is in general a function of ψ_n, ψ_n^*, u_n, and u_n^*.

Since the amplitude ϕ_n and its complex conjugate ϕ_n^* both are involved in Eq. (3) we have to consider two different

frequency components $(\omega \pm p)$ in u_n. In particular we assume

$$u_n = a_n e^{-i(\omega+p)t} + b_n e^{-i(\omega-p)t}, \tag{4}$$

where a_n and b_n correspond to two different channels in the scattering process. Substituting Eq. (4) in Eq. (3) and considering the coefficients of $e^{-i(\omega+p)t}$ and $e^{-i(\omega-p)t}$ separately, we obtain a pair of coupled equations for a_n and b_n. A single iterative relation can replace those equations and can be written as

$$E_n Y_n + I(Y_{n+1} + Y_{n-1}) = 0. \tag{5}$$

Here, Y_n is an amplitude vector and I, E_n are matrices of the same order as Y_n. In particular I is an identity matrix. The explicit forms of g, E_n, and Y_n depend on the specific form of f defined in Eq. (1). We will present these functional forms in Sec. IV where we shall discuss phonon-breather scattering in the DNLS model in detail. On the other hand from Eq. (5) we obtain a recursive relation

$$\begin{pmatrix} Y_n \\ Y_{n-1} \end{pmatrix} = M_n \begin{pmatrix} Y_{n+1} \\ Y_n \end{pmatrix}, \quad \text{with } M_n = \begin{pmatrix} 0 & I \\ -I & -E_n \end{pmatrix}. \tag{6}$$

Here, M_n is a unimodular square matrix (and moreover this is an area preserving mapping). Equation (6) can be taken as representing the dynamics of the scattering process since repeated applications of it relate the amplitudes of the incoming and the outgoing waves. The amplitudes at the source $(n=-N)$ and at the receiving points $(n=N)$ for phonons are related to each other as

$$\begin{pmatrix} Y_{-N} \\ Y_{-N-1} \end{pmatrix} = M \begin{pmatrix} Y_{N+1} \\ Y_N \end{pmatrix}, \tag{7}$$

where we assume that N is sufficiently large, so that the source is far away from the breather center, and the product matrix M (square) is defined as

$$M = M_{-N} M_{-N+1} \cdots M_{-1} M_0 M_1 \cdots M_{N-1} M_N. \tag{8}$$

Therefore, once we are able to construct the transfer matrix M, we can find the reflection coefficient (R) or the ratio of the reflected to incident flux of energy and the transmission coefficient (T) or the ratio of the transmitted to incident flux of energy. Quite clearly the matrix M is invertible. Also from the fact that in a regular lattice the left- and the right-hand sides with respect to the breather center are equivalent we can say that M will be *symplectic* in nature, which implies that M is antisymmetric and nondegenerate and obviously invertible.

III. SUMMARY OF RESULTS FOR THE ON-SITE MONOCHROMATIC DISCRETE BREATHER SOLUTIONS IN THE PWS VERSION OF THE DNLS MODEL AND ITS STABILITY ANALYSIS

In [15] authors presented exact analytical results for the construction of one-site monochromatic breathers in the PWS version of the DNLS model, and its stability analysis is presented in [16]. In this section we briefly discuss the main results of those works.

The force function in this particular model as represented by the last term in Eq. (1) is

$$f(|\psi_n|) = \gamma\left(1 - \frac{a}{|\psi_n|}\right)\Theta(|\psi_n| - a), \tag{9}$$

where γ, Θ, and a are the strength of nonlinearity, the Heaviside step function, and the threshold parameter of the nonlinearity, respectively. All these parameters and the wave function ψ_n are scaled appropriately such that $a=1$, and all of them become dimensionless. The Heaviside step function is defined such that when $|\psi_n| > a$ $(=1)$, $\Theta(|\psi_n| - a) = 1$; otherwise, it is zero. Combining Eqs. (1) and (9) the PWS version of the DNLS model becomes

$$i\dot{\psi}_n + V(\psi_{n+1} + \psi_{n-1}) + \gamma\left(1 - \frac{1}{|\psi_n|}\right)\Theta(|\psi_n| - 1)\psi_n = 0$$
$$(n = 0, \pm 1, \pm 2, \ldots). \tag{10}$$

Assuming kink-antikink type (bright breather) of localized solutions [see Eq. (2)] admitted by the above equation, the following mapping has been arrived with scaled variables $\frac{\omega}{V} \to \omega$ and $\frac{\gamma}{V} \to \gamma$:

$$\phi_{n+1} + \phi_{n-1} + \omega\phi_n + \gamma[\phi_n - \mathrm{sgn}(\phi_n)]\Theta(|\phi_n| - 1) = 0. \tag{11}$$

This can be expressed as a 2D mapping. The PWS version of the DNLS model enables one to construct the *homoclinic trajectory* associated with a *hyperbolic fixed point* of the mapping exactly. The breather trajectory can be related to a homoclinic orbit of the mapping by choosing the breather to be centered at $n=0$. Following this approach one is able to construct the trajectory of the monochromatic breather solution as

$$\phi_n = \frac{\gamma\lambda^{|n|}}{\gamma + \lambda - \frac{1}{\lambda}}, \quad |\lambda| < 1, \tag{12}$$

where λ is the spatial decay rate of the breather profile defined as

$$\omega = -\left(\lambda + \frac{1}{\lambda}\right). \tag{13}$$

The boundary conditions $(\phi_0 > 1$ and $\phi_{\pm 1} < 1)$ imply that the necessary conditions for the existence of the breather solution require

$$|\gamma| > 1 + \frac{1}{|\lambda|}, \quad \gamma\omega < 0. \tag{14}$$

In other words for any given breather frequency ω outside the linear band and γ satisfying Eq. (14) an exact breather solution to the PWS version of the DNLS equation has been obtained [following Eq. (2)] and is given by [15]

$$\psi_n = \frac{\gamma\lambda^{|n|}}{\gamma + \lambda - \frac{1}{\lambda}} e^{-i\omega t}. \tag{15}$$

Now from Eqs. (14) and (15), Fig. 1, and also from the fact that $|\psi_n| = |\phi_n|$, we observe that the PWS model (in the common region of overlap in between 1 and 2 as mentioned earlier) follows the cubic one provided $n < 1$.

The linear stability analysis (see [16]) of the breather solution given by Eq. (15) has been studied against a small perturbation

$$u_n(t) = x_n(t) + iy_n(t), \tag{16}$$

where $x_n(t)$ and $y_n(t)$ are real and small, and are such as to satisfy a pair of coupled differential equations,

$$\ddot{X} = AY, \tag{17a}$$

$$\ddot{Y} = A^T X, \tag{17b}$$

with $X = (\ldots, x_{-2}, x_{-1}, x_0, x_1, x_2, \ldots)^T$, $Y = (\ldots, y_{-2}, y_{-1}, y_0, y_1, y_2, \ldots)^T$, and A being a banded matrix. The eigenvalues μ of A are related to the growth rate of perturbations (P) through $\mu = P^2$ and can be real negative or real positive or complex. The breather is linearly stable when μ is negative, while for the latter two cases it will be unstable. The real and negative eigenvalues of A may be associated with either localized or extended eigenmodes. The eigenvalues corresponding to the extended eigenmodes form a band

$$(2\cos\theta + \omega)^2 + \mu = 0, \quad 0 \le \theta \le \pi. \tag{18}$$

It implies that the band extends from $-(\omega+2)^2$ to $-(\omega-2)^2$. In addition each eigenvalue μ in the interior of the band ($0 < \theta < \pi$) is doubly degenerate, while for a given λ the band edges are empty except when γ satisfies (for the inner band edge, $\theta = 0$)

$$\gamma = \gamma_1(\lambda) = \frac{(\lambda - \lambda^{-1})\sqrt{(\lambda + \lambda^{-1})^2 - 2(\lambda + \lambda^{-1})}}{(\lambda - \lambda^{-1}) + \sqrt{(\lambda + \lambda^{-1})^2 - 2(\lambda + \lambda^{-1})}}, \tag{19}$$

and similarly for the outer band edge, $\theta = \pi$,

$$\gamma = \gamma_2(\lambda) = \frac{(\lambda - \lambda^{-1})\sqrt{(\lambda + \lambda^{-1})^2 + 2(\lambda + \lambda^{-1})}}{(\lambda - \lambda^{-1}) + \sqrt{(\lambda + \lambda^{-1})^2 + 2(\lambda + \lambda^{-1})}}. \tag{20}$$

In that case the band is occupied by a single symmetric localized mode. After the appearance of the localized mode, as γ is continued to vary from below, this localized mode approaches the origin $\mu = 0$ in the eigenspace, and finally the breather gets destabilized as μ touches the origin.

IV. PHONON SCATTERING BY DISCRETE BREATHERS IN DNLS MODEL

The extensive use of the DNLS model in the literature is due to the fact that it is found to arise in many physical contexts. In one-dimensional systems the model is represented by Eq. (1). The DNLS model admits different types of solutions. But we are looking for a typical solution known as discrete breathers. Starting from the anti-integrable limit (also known as anticontinuous limit), MacKay and Aubry [25] first proved the existence of breather solution in an infinite chain of anharmonic lattices. Instead of the usual cubic type of nonlinearity, a PWS function has been chosen to represent the nonlinearity. In this particular version of the DNLS model, as discussed earlier [15,16], we present exact analytical expressions for one- and two-site (antiphase) DB solutions with their linear stability analysis. To study the phonon scattering by DBs we first apply a small perturbation $u_n(t)$ to the breather solution [Eq. (1)] and study the asymptotic behavior of $u_n(t)$, provided the perturbation is allowed to evolve for a sufficiently long time. The perturbed solution becomes

$$\psi_n(t) = \overline{\psi_n}(t) + u_n(t), \tag{21}$$

where $\overline{\psi_n}(t) = \phi_n e^{-i\omega t}$ is the unperturbed solution. Applying Eq. (21) in Eq. (1) and after linearization we obtain the time-evolution equation for the perturbation as

$$i\dot{u}_n(t) + (u_{n+1} + u_{n-1}) + \gamma\left[\left(1 - \frac{1}{|\phi_n|}\right)u_n + \frac{\phi_n}{2|\phi_n|}\left(\frac{u_n}{\phi_n} + \frac{u_n^*}{\phi_n^*}e^{-2i\omega t}\right)\right]\Theta(|\phi_n| - 1) = 0. \tag{22}$$

We have used the scaled variables $\frac{\chi}{V} \to \gamma$ and $\frac{\omega}{V} \to \omega$, and the wave function ψ_n is normalized in such a fashion that the threshold parameter becomes unity ($a = 1$). Now substituting Eq. (4) in Eq. (22), expanding it, and equating the real and imaginary parts to zero separately, we obtain

$$(\omega + p)a_n + (a_{n+1} + a_{n-1}) + \gamma\left[\left(1 - \frac{1}{2|\phi_n|}\right)a_n + \frac{1}{2|\phi_n|}b_n^*\right]\Theta(|\phi_n| - 1) = 0, \tag{23a}$$

$$(\omega - p)b_n + (b_{n+1} + b_{n-1}) + \gamma\left[\left(1 - \frac{1}{2|\phi_n|}\right)b_n + \frac{1}{2|\phi_n|}a_n^*\right]\Theta(|\phi_n| - 1) = 0. \tag{23b}$$

These are two coupled equations for a_n and b_n corresponding to two different scattering channels (channels are pathways for plane waves; if the frequency of the wave is inside the linear spectrum, it is called an open channel; otherwise, it is a closed channel) in our scattering analysis. In the asymptotic regions (in our analysis it is the region with $|n| > 1$) Eqs. (23a) and (23b) decouple and yield [as Eq. (15) suggests, $|\phi_n| < 1$ in this region]

$$(\omega + p)a_n + a_{n+1} + a_{n-1} = 0, \tag{24a}$$

$$(\omega - p)b_n + b_{n+1} + b_{n-1} = 0. \tag{24b}$$

The asymptotic solutions corresponding to those channels are $a_n \sim e^{iq_a n}$ and $b_n \sim e^{iq_b n}$; hence,

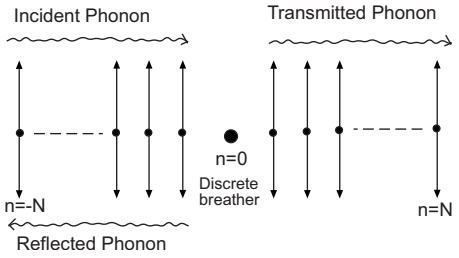

FIG. 2. Schematic for phonon transmission by discrete breathers.

$$\cos q_a = -\frac{\omega + p}{2}, \tag{25a}$$

$$\cos q_b = -\frac{\omega - p}{2}, \tag{25b}$$

where q_a and q_b are the wave vectors corresponding to those channels. These asymptotic solutions are either traveling modes (with velocity $\frac{|p \pm \omega|}{q}$) or growing (decaying) modes. For traveling modes, both q_a and q_b are real, and hence $|\frac{\pm p-\omega}{2}| \leq 1$. If on the other hand one channel is traveling (say that corresponding to a_n) and the other channel is decaying (or growing), q_a is real while q_b imaginary implies $|\frac{-p-\omega}{2}| \leq 1$ and $|\frac{p-\omega}{2}| > 1$, and vice versa. To describe the scattering process we consider a chain of $(2N+1)$ lattice sites where $n=-N$ and $n=N$ are the source and target points, respectively. To construct the transfer matrix for the said process (see Fig. 2) we first define an amplitude vector Y_n as

$$Y_n = (a_n, b_n^*)^T. \tag{26}$$

Using this vector we can replace Eqs. (23a) and (23b) with a recursive relation as defined in Eq. (5) where I is a 2×2 identity matrix and E_n is another 2×2 matrix involving the parameters γ, p, ω of the model, respectively. From Eq. (5) we obtain the same recursive relation as Eq. (6) with

$$E_n = \begin{pmatrix} p + \omega + \eta & \dfrac{\eta}{2b-1} \\ \dfrac{\eta}{2b-1} & -p + \omega + \eta \end{pmatrix}, \tag{27}$$

where $\eta = \gamma(1 - \frac{1}{2b})\Theta(|\phi_n| - 1)$, ω is the breather frequency, and

$$b = |\phi_0| = \frac{\gamma}{\gamma + \lambda - \dfrac{1}{\lambda}} \tag{28}$$

is the breather amplitude at the lattice site $n=0$. Repeated applications of Eq. (6) over the entire chain of $(2N+1)$ lattice sites obtain an equation similar to Eq. (7).

Since the asymptotic behavior of the channels for a_n and b_n is either a traveling or a growing (decaying) mode, the general solutions for a_n and b_n can be written as

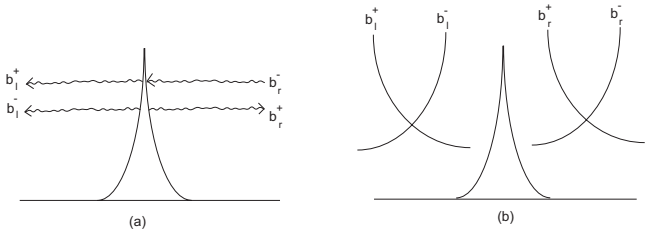

FIG. 3. Configuration of phonon transmission by discrete breathers in traveling mode for (a) real q_b and that in growing (decaying) mode for (b) imaginary q_b.

$$a_n = a_l^+ e^{iq_a n} + a_l^- e^{-iq_a n}, \quad b_n = b_l^+ e^{iq_b n} + b_l^- e^{-iq_b n}, \quad \text{for } n \to -\infty, \tag{29a}$$

$$a_n = a_r^+ e^{iq_a n} + a_r^- e^{-iq_a n}, \quad b_n = b_r^+ e^{iq_b n} + b_r^- e^{-iq_b n}, \quad \text{for } n \to \infty, \tag{29b}$$

where the coefficients $a_l^{\pm}, a_r^{\pm}, b_l^{\pm}, b_r^{\pm}$ are small. Here, the subscripts l and r indicate left and right sides with respect to the breather center (see Fig. 3), respectively. Substituting Eqs. (29a) and (29b) in Eq. (7) we obtain,

$$\begin{pmatrix} a_l^+ e^{-iq_a N} + a_l^- e^{iq_a N} \\ (b_l^+)^* e^{iq_b^* N} + (b_l^-)^* e^{-iq_b^* N} \\ a_l^+ e^{-iq_a (N+1)} + a_l^- e^{iq_a (N+1)} \\ (b_l^+)^* e^{iq_b^* (N+1)} + (b_l^-)^* e^{-iq_b^* (N+1)} \end{pmatrix} = M \begin{pmatrix} a_r^+ e^{iq_a (N+1)} + a_r^- e^{-iq_a (N+1)} \\ (b_r^+)^* e^{-iq_b^* (N+1)} + (b_r^-)^* e^{iq_b^* (N+1)} \\ a_r^+ e^{iq_a N} + a_r^- e^{-iq_a N} \\ (b_r^+)^* e^{-iq_b^* N} + (b_r^-)^* e^{iq_b^* N} \end{pmatrix}, \tag{30}$$

where M is a 4×4 square matrix. The elements of that matrix involve the parameters γ, p, ω, and b $(=\phi_0)$. We obtain four linear independent equations from Eq. (30).

From Eqs. (29a) and (29b) we observe that if both channels for a_n and b_n are traveling modes, both q_a and q_b are real and all eight scattering coefficients need not be zero. Four more constraints are necessary to satisfy a unique solution on the four-dimensional solution set. These constraints specify a particular scattering configuration. For example, if the amplitudes for the incoming phonons from the left and the right sides of the DB through two channels, a_l^+, b_l^+, a_r^-, and b_r^-, are given, the amplitudes of the outgoing phonons, a_l^-, b_l^-, a_r^+, and b_r^+, will be determined uniquely by four independent equations in Eq. (30). In this bichannel scattering process two different frequencies are involved as seen from Eq. (4). On the other hand for the NDKG model we may have as many as infinite scattering channels and also the outgoing waves have different harmonic frequencies compared to the breather frequency [26]. In other words the inelastic effect can be observed. In such cases the total incident flux of energy is less than the total outgoing flux of energy. In a closed system there is no such incident energy from outside to the breather except the incident phonon energy; hence, this ex-

cess amount of energy comes from the breather itself. As a result the breather will gradually lose energy and decay thereby.

If only one channel, say a_n, is a traveling mode, q_a is real and q_b is imaginary. Then the coefficients for the exponentially growing parts of the asymptotic solution should be zero for a physical solution, i.e., $b_r^-=0$ and $b_l^+=0$. This provides two more constraints; hence, a 2D solution set can be obtained thereby. Let a_l^+ and a_r^- are given; hence, we can determine a_l^- and a_r^+ uniquely. Similar set of results can be obtained for b_n as the only traveling channel. This type of scattering happens to be elastic by nature and satisfies energy conservation relation.

If on the other hand neither a_n nor b_n is traveling we must have both q_a and q_b imaginary. We may call this situation as zero-scattering channel. Hence, $a_r^-=b_r^-=a_l^+=b_l^+=0$ (as now they are the coefficients of exponentially growing solutions in the asymptotic region). So we can solve Eq. (30) for the other four coefficients uniquely. If instead we consider that the channel for a_n have only the exponentially decaying parts (i.e., $a_l^+=a_r^-=0$) then we may consider the scattering property of the b_n channel in the nontraveling region. The two other constraint conditions [which are the basic need for the solution of Eq. (30) as mentioned earlier] that we consider are the various scattering configurations of the b_n channel in the nontraveling mode, namely, *growing*, *decaying*, PT, and PR modes.

In the analysis to follow we mainly consider the single-channel scattering process (elastic) in the traveling phonon mode and determine exact analytical expression for the transmission coefficient (T), complemented by the numerical simulation. Similar analysis can be done for the other two scattering configurations staring from Eq. (30), hence yielding the expression for T. Nevertheless, for our present analysis we kept one channel open while the other is closed and show that the analysis can be done quite easily in the PWS version of the nonlinearity which we are considering throughout our previous analysis. In particular we assume that the b_n channel is open and a_n is closed. Also let the wave be incident from the left-hand side of the DB center. In that case b_l^+ is known and $b_r^-=0$. For the closed channel since the coefficients of the exponentially growing (decaying) mode is zero, hence, $a_l^+=a_r^-=0$. Further assuming the amplitude of the incident wave along the channel for b_n as unity, the scattering configuration in this case finally corresponds to $b_l^+=1$, $b_r^-=0$, $a_l^+=0$, $a_r^-=0$. We therefore have four constraints. These constraints together with the four independent equations obtained form Eq. (30) determine a unique solution. Taking this configuration we can rewrite Eq. (30) as

$$\begin{pmatrix} a_l^- e^{iq_a N} \\ e^{iq_b^* N} + (b_l^-)^* e^{-iq_b^* N} \\ a_l^- e^{iq_a (N+1)} \\ e^{iq_b^* (N+1)} + (b_l^-)^* e^{-iq_b^* (N+1)} \end{pmatrix} = M \begin{pmatrix} a_r^+ e^{iq_a (N+1)} \\ (b_r^+)^* e^{-iq_b^* (N+1)} \\ a_r^+ e^{iq_a N} \\ (b_r^+)^* e^{-iq_b^* N} \end{pmatrix}. \tag{31}$$

For a symplectic *unimodular area preserving mapping* M_n as defined by Eq. (6) and also from the nature of Y_n [as defined by Eq. (26)] we observe that each of $0, I, E_n$ is of order 2×2, where 0 is a null matrix and I is the identity matrix. From Eq. (9) M is a product of $2N+1$ M_n like matrices. Let us evaluate M for some typical values of N.

When $N=1$ we have $M=M_1M_0M_1$. Hence,

$$M = \begin{pmatrix} 0 & I \\ I & -E_1 \end{pmatrix} \begin{pmatrix} 0 & I \\ I & -E_0 \end{pmatrix} \begin{pmatrix} 0 & I \\ I & -E_1 \end{pmatrix} = \begin{pmatrix} S_{11} & S_{12} \\ -S_{12} & S_{22} \end{pmatrix}. \tag{32}$$

It can be easily shown that $\det(M)=1$.

Again for $N=2$ we have $M=M_2M_1M_0M_1M_2$. Hence,

$$M = \begin{pmatrix} 0 & I \\ I & -E_2 \end{pmatrix} \begin{pmatrix} S_{11} & S_{12} \\ -S_{12} & S_{22} \end{pmatrix} \begin{pmatrix} 0 & I \\ I & -E_2 \end{pmatrix} = \begin{pmatrix} S'_{11} & S'_{12} \\ -(S'_{12})^t & S'_{22} \end{pmatrix}. \tag{33}$$

Explicit calculation again shows $\det(M)=1$. Therefore, M is a unimodular and symplectic matrix with real elements as stated earlier. Again as M is a 4×4 matrix with nonzero elements along the two principal diagonals the combined operations (addition, subtraction, and multiplication) of any number of E_n's will have the same structure. This implies that for any N, M can be written as given by Eq. (33) where S_{ij} is a 2×2 matrix with nonzero elements and with $(S_{ij})^t$ being its transpose. Hence,

$$M = \begin{pmatrix} M_{11} & M_{12} & M_{13} & M_{14} \\ M_{21} & M_{22} & M_{23} & M_{24} \\ -M_{13} & -M_{23} & M_{33} & M_{34} \\ -M_{14} & -M_{24} & M_{43} & M_{44} \end{pmatrix}. \tag{34}$$

Here, M_{ij} is simply the notation of the elements of the product matrix M as represented by Eq. (8).

With the scattering configuration mentioned earlier we have obtained the following set of four equations obtained from Eqs. (31) and (34):

$$a_l^- e^{iq_a N} = a_r^+ e^{iq_a N}(M_{11}e^{iq_a} + M_{13}) + (b_r^+)^* e^{-iq_b^* N}(M_{12}e^{-iq_b^*} + M_{14}), \tag{35a}$$

$$e^{-iq_b N} + b_l^- e^{iq_b N} = b_r^+ e^{iq_b N}(M_{22}e^{iq_b} + M_{24}) + (a_r^+)^* e^{-iq_a^* N}(M_{21}e^{-iq_a^*} + M_{23}), \tag{35b}$$

$$a_l^- e^{iq_a (N+1)} = a_r^+ e^{iq_a N}(-M_{13}e^{iq_a} + M_{33}) + (b_r^+)^* e^{-iq_b^* N}(-M_{23}e^{-iq_b^*} + M_{34}), \tag{35c}$$

$$e^{-iq_b (N+1)} + b_l^- e^{iq_b (N+1)} = b_r^+ e^{iq_b N}(-M_{24}e^{iq_b} + M_{44}) + (a_r^+)^* e^{-iq_a^* N}(-M_{14}e^{-iq_a^*} + M_{43}). \tag{35d}$$

Since the a_n channel is closed while b_n is kept open, we have q_a imaginary and q_b real. From Eqs. (35a)–(35d), with $iq_a^*=k_a$ for real k_a and with the scaling $b_l^+=1$ we obtain

$$b_r^+ = \frac{e^{-2iq_bN}(1-e^{-2iq_b})\alpha_1}{\alpha_1\alpha_2+\alpha_3\alpha_4}, \tag{36}$$

where

$$\alpha_1 = M_{11}e^{-k_a} + 2M_{13} - M_{33}e^{k_a}, \tag{37a}$$

$$\alpha_2 = M_{22}e^{iq_b} + 2M_{24} - M_{44}e^{-iq_b}, \tag{37b}$$

$$\alpha_3 = (-M_{23}e^{iq_b} + M_{34})e^{k_a} - (M_{12}e^{iq_b} + M_{14}), \tag{37c}$$

$$\alpha_4 = (M_{14}e^{-iq_b} + M_{21})e^{-k_a} + (M_{23} - M_{43}e^{-iq_b}). \tag{37d}$$

Similarly

$$b_l^- = -e^{-2iq_bN}\left(\frac{\alpha_3^*}{\alpha_3}\right) + \frac{b_r^+e^{k_a}e^{iq_b}}{\alpha_3}(-\alpha_2'\alpha_4'' + \alpha_2''\alpha_4'), \tag{38}$$

where

$$\alpha_2' = M_{22}e^{iq_b} + M_{24}, \tag{39a}$$

$$\alpha_2'' = M_{24} - M_{44}e^{-iq_b}, \tag{39b}$$

$$\alpha_4' = M_{14}e^{-iq_b}e^{-k_a} - M_{43}e^{-iq_b}, \tag{39c}$$

$$\alpha_4'' = M_{21}e^{-k_a} + M_{23}, \tag{39d}$$

such that

$$\alpha_2 = \alpha_2' + \alpha_2'', \tag{40a}$$

$$\alpha_4 = \alpha_4' + \alpha_4''. \tag{40b}$$

Now, by definition, the transmission and reflection coefficients are

$$T = \left|\frac{b_r^+}{b_l^+}\right|^2 = \left|\frac{e^{-2iq_bN}(1-e^{-2iq_b})\alpha_1}{\alpha_1\alpha_2+\alpha_3\alpha_4}\right|^2, \tag{41}$$

$$R = \left|\frac{b_l^-}{b_l^+}\right|^2 = \left|-e^{-2iq_bN}\left(\frac{\alpha_3^*}{\alpha_3}\right) + \frac{b_r^+e^{k_a}}{\alpha_3}e^{iq_b}(-\alpha_2'\alpha_4'' + \alpha_2''\alpha_4')\right|^2. \tag{42}$$

The exact expressions for T and R depend on the explicit form of α_i's.

Now with reference to Eq. (8) taking $N=1$ the elements M_{ij} of Eq. (34) are $M_{11}=x_0$, $M_{12}=z_0=M_{21}$, $M_{13}=-1+x_0x_1$, $M_{14}=z_0y_1$, $M_{22}=y_0$, $M_{24}=-1+y_0y_1$, $M_{23}=z_0x_1$, $M_{33}=2x_1-x_0x_1^2$, $M_{34}=-x_1y_1z_0=M_{43}$, and $M_{44}=2y_1-y_0y_1^2$, where $x_0=p+\omega+\Gamma$, $x_n(n\neq 0)=p+\omega$, $y_0=-p+\omega+\Gamma$, $y_n(n\neq 0)=-p+\omega$, $z_0=\frac{\gamma}{2b}$, and $z_n(n\neq 0)=0$. Again with the aid of Eqs. (37a)–(37d) and (39a)–(39d) and the matrix elements mentioned above, we obtain $\alpha_1=e^{3k_a}(2\sinh k_a+\Gamma)$, $\alpha_2=e^{3iq_b}(2i\sin q_b+\Gamma)$, $\alpha_3=-\frac{\gamma}{2b}e^{2k_a-iq_b}$, $\alpha_4=\frac{\gamma}{2b}e^{k_a-2iq_b}$, $\alpha_2'=(2\cos q_b-\Gamma)e^{-iq_b}-1$, and $\alpha_4''=-\frac{\gamma}{2b}e^{k_a}$.

Hence, using Eqs. (40a), (40b), and (41) we can simply derive

$$T = \frac{4\sin^2 q_b}{(\Gamma-H)^2+4\sin^2 q_b}, \tag{43}$$

$$R = \frac{(\Gamma-H)^2}{(\Gamma-H)^2+4\sin^2 q_b}, \tag{44}$$

where

$$\Gamma = \gamma\left(1-\frac{1}{2b}\right), \tag{45a}$$

$$H = \frac{\left(\frac{\gamma}{2b}\right)^2}{e^{-k_a}-e^{k_a}+\Gamma}, \tag{45b}$$

$$e^{k_a}-e^{-k_a} = 2(\cos q_b+\omega+1)^{1/2}(\cos q_b+\omega-1)^{1/2}. \tag{45c}$$

The last equation [Eq. (45c)] has been derived from Eqs. (25a) and (25b) by noting that

$$e^{k_a}+e^{-k_a} = -(p+\omega) = -(2\cos q_b+2\omega). \tag{46}$$

Equations (43) and (44) clearly show that

$$R+T=1. \tag{47}$$

Hence, the sum of the reflected and the transmitted fluxes of energy is equal to the incident flux of energy, which is nothing but the energy conservation relation. Hence, as we have mentioned earlier the energy conservation holds well in the case of single-channel scattering.

Similar calculations for $N=2$ [referring to Eq. (8) again] show that $M_{11}=-2x_1+x_0x_1^2$, $M_{12}=x_1y_1z_0=M_{21}$, $M_{13}=1-x_0x_1-x_1^2(2-x_0x_1)+x_1y_1z_1z_0$, $M_{14}=z_0x_1(y_1^2-1)-z_1x_1(2-x_0x_1)$, $M_{22}=-2y_1+y_0y_1^2$, $M_{24}=1-y_0y_1-y_1^2(2-y_0y_1)+x_1y_1z_1z_0$, $M_{23}=z_0y_1(x_1^2-1)-y_1z_1(2-y_0y_1)$, $M_{33}=-x_0+2x_1(-1+x_0x_1)+x_1^3(2-x_0x_1)$, $M_{34}=z_0(-1+2x_1y_1-x_1^2y_1^2)=M_{43}$, and $M_{44}=-y_0+2y_1(-1+y_0y_1)+y_1^3(2-y_0y_1)$, and we have $\alpha_1=e^{5k_a}(2\sinh k_a+\Gamma)$, $\alpha_2=e^{-3iq_b}(2i\sin q_b+\Gamma)$, $\alpha_3=-4\sinh k_a\cos q_be^{3k_a-2iq_b}\frac{\gamma}{2b}$, $\alpha_4=4\sinh k_a\cos q_be^{2k_a-3iq_b}\frac{\gamma}{2b}$, $\alpha_2'=2(1+\Gamma\cos q_b-2\cos^2 q_b)(3+2e^{2iq_b}-4\cos^2 q_b)-1$, and $\alpha_4''=-2\cos q_b\frac{\gamma}{2b}(-2\cos q_ae^{-k_a}+4\cos^2 q_a-1)$. Using this set of α_i's we again obtain Eqs. (41) and (42). We can generalize the above results, namely, $N=1$ and $N=2$ for the entire lattice by using the property of the PWS version of nonlinearity. Equations (29a) and (29b) clearly indicate that the solution is plane wave by nature. Again Eq. (12) shows that the breather amplitude varies with n as $\lambda^{|n|}$. Even for values of n slightly greater than 1 the amplitude rapidly decays and heads toward zero. So we can say that as $n>1$ we will enter the asymptotic region where the behavior of the solution is independent of the lattice site.

We now study the cases of perfect transmission and reflection with the aid of Eqs. (43) and (44). The first of those equations suggests that under the limit $\Gamma-H\to 0$ we may have a perfect transmission. In order to evaluate that particular limit we use Eqs. (45a)–(45c), (13), and (28). As a consequence we obtain

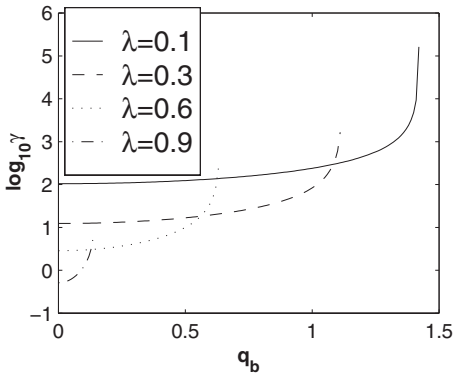

FIG. 4. $\log_{10}\gamma$ vs wave vector q_b plot (because of large variations in γ even for a very small change in q_b) at PT keeping λ as a parameter ($\lambda=0.1,0.3,0.6,0.9$) following Eq. (49) within the range $0\leq q_b\leq\frac{\pi}{2}$.

$$\gamma^2\left(1-\frac{1}{2b}\right)^2-\left(\frac{\gamma}{2b}\right)^2=2\gamma\left(1-\frac{1}{2b}\right)(\cos q_b-\lambda-\lambda^{-1}+1)^{1/2}(\cos q_b-\lambda-\lambda^{-1}-1)^{1/2}. \tag{48}$$

Hence,

$$\gamma=\frac{(\lambda-\lambda^{-1})(\cos q_b-\lambda-\lambda^{-1}+1)^{1/2}(\cos q_b-\lambda-\lambda^{-1}-1)^{1/2}}{(\lambda-\lambda^{-1})+(\cos q_b-\lambda-\lambda^{-1}+1)^{1/2}(\cos q_b-\lambda-\lambda^{-1}-1)^{1/2}}. \tag{49}$$

Taking now the limits $q_b\to 0$ and $q_b\to\pi$, respectively, in Eq. (49) we obtain

$$\gamma|_{q_b\to 0}=\frac{(\lambda-\lambda^{-1})\sqrt{(\lambda+\lambda^{-1})^2-2(\lambda+\lambda^{-1})}}{(\lambda-\lambda^{-1})+\sqrt{(\lambda+\lambda^{-1})^2-2(\lambda+\lambda^{-1})}}, \tag{50a}$$

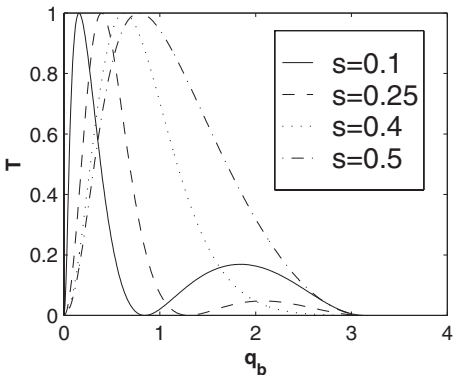

FIG. 5. Transmission coefficient T vs wave vector q_b plot for a set of different γ values keeping $\lambda=0.5$ (constant). The γ values are chosen with the help of Eq. (49) by taking $q_b=s\pi/2$, where different s values are mentioned in the legend. The corresponding γ values are 4.6559, 6.4861, 14.9964, and 187.7064. Numerical data support that the perfect transmission points ($T=1$) in the graph are indeed obtained at $q_b=s\pi/2$. Also for $s=0.1$ and $s=0.25$ we have $q_b=0.8410$ and $q_b=1.2610$ at which $T=0$, again supported by Eq. (54) with $\gamma=4.6559$, and $\gamma=6.4861$ and $\lambda=0.5$.

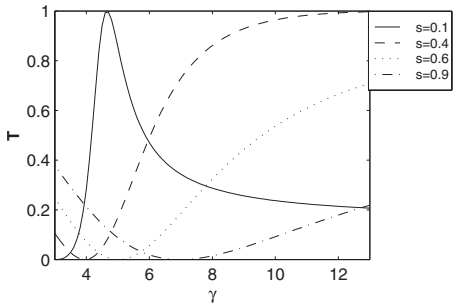

FIG. 6. Transmission coefficient T vs nonlinear parameter γ plot for $\lambda=0.5$ and for $q_b=s\pi/2$ with s values mentioned in the legend. The γ values at which PT occurs can be calculated again with the aid of Eq. (49) and also can be verified from the numerical data; in fact $\gamma=4.7$ for $s=0.1$ and $\gamma=13$ for $s=0.4$. Again $T=0$ for $\gamma=3$, $\gamma=4$, $\gamma=5$, $\gamma=7$ corresponding to $s=0.1$, $s=0.4$, $s=0.6$, $s=0.9$, respectively, verified both from numerical data and Eq. (54).

$$\gamma|_{q_b\to\pi}=\frac{(\lambda-\lambda^{-1})\sqrt{(\lambda+\lambda^{-1})^2+2(\lambda+\lambda^{-1})}}{(\lambda-\lambda^{-1})+\sqrt{(\lambda+\lambda^{-1})^2+2(\lambda+\lambda^{-1})}}. \tag{50b}$$

In the stability analysis of one-site monochromatic DB solution in the PWS version of the DNLS model given by Eqs. (1) and (9) (see [16]), it is shown that as the nonlinear parameter γ is made to vary from below or above one can encounter a situation where for a certain value of γ (keeping the other parameters fixed) a localized mode starts to appear at the band edge of the extended eigenmodes. Hence, comparing Eqs. (50a) and (50b) with Eqs. (19) and (20) we can say that perfect transmission happens to appear at the threshold of a localized mode (LM), which occurs at the band edge of the extended eigenmodes. Taking now the limit $q_b\to\frac{\pi}{2}$ in Eq. (49) again we may have

$$\gamma|_{q_b\to\pi/2}=\frac{(\lambda-\lambda^{-1})\sqrt{(\lambda+\lambda^{-1})^2-1}}{(\lambda-\lambda^{-1})+\sqrt{(\lambda+\lambda^{-1})^2-1}}, \tag{51}$$

which determines the condition of getting PT at the band center. In a similar way we can obtain the relation between γ and λ at perfect transmission for any q_b, but in doing that we also have to keep in mind the breather existence criteria mentioned in Eq. (14). Figure 4 depicts the ranges of variations of γ against q_b at perfect transmission for various λ's. The

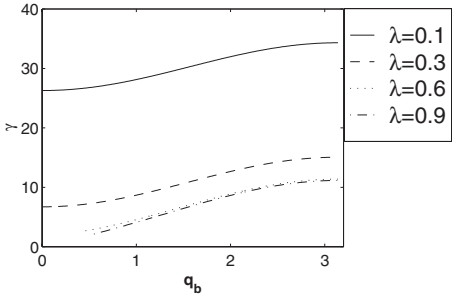

FIG. 7. Nonlinear parameter γ vs wave vector q_b plot at perfect reflection for four different values of λ, namely, 0.1, 0.3, 0.6, and 0.9.

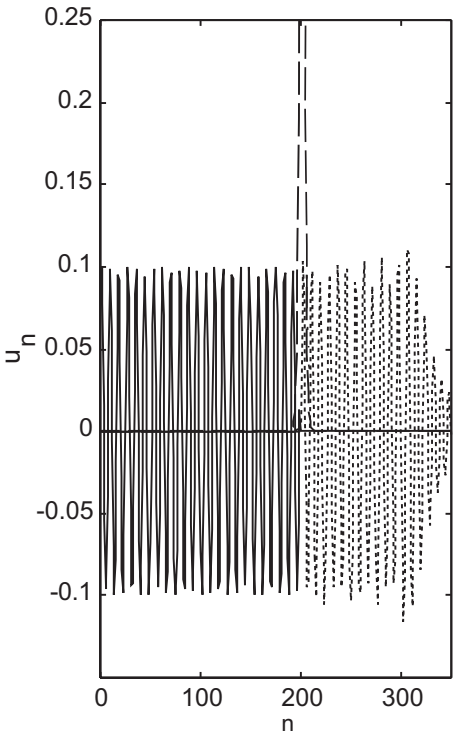

FIG. 8. In the figure the solid line in the left and the dotted line in the right indicate the incident and transmitted waves, respectively. Also the dashed line in the middle indicates the breather itself. The figure shows $T\to 1$ (transmitted amplitude becomes almost equal to incident wave amplitude) for $\lambda=0.5$, $q_b=0.1\pi/2$, and $\gamma=4.6559$ with the aid of Fig. 5 and for a time period of $t=12$. Again using Eqs. (13) and (25b) and with the above q_b and λ we obtain $p=2\cos q_b+\omega=-0.5246$, and the velocity of the wave is given by $V=|p-\omega|/q_b=12.57$. Hence, during the time interval chosen the wave advances through a distance of $Vt=150.89$. Also from the figure it is clearly evident that there is no reflected wave at all.

sign(s) and minimum value(s) of γ follow as a consequence of Eq. (14). The plots are done only for the positive values of λ. It is clearly seen from Fig. 4 that PT can only be obtained within the range $q_b=0$ to $q_b=\pi/2$. Similar set of plots can also be done for negative values of λ as well, where we can obtain PT for the other half of the wave vector, namely, $q_b=\pi/2$ to $q_b=\pi$.

After analyzing the behavior of the parameters at PT we shall now study Fig. 5 where the nature of variation of T with q_b for different γ's in the channel for b_n when the channel for a_n is kept closed is shown. It is straightforward from Fig. 5 that only for a definite γ we can have perfect transmission at a definite q_b. The numerical data show that a particular γ follows from Eq. (49) with a properly chosen λ and the corresponding q_b. Hence, we may conclude that only phonons of a particular frequency depending on λ and γ can pass through the breather with unmodified amplitude. All other phonons not having that particular frequency will be either blocked by the breather or their amplitudes will be somewhat diminished after transmission. The figure also reveals that at some definite frequencies (as mentioned in Fig. 5) the DB behaves as opaque to the incident photons. Those zero transmission points obviously indicate perfect reflection, which is again verified by Eq. (54).

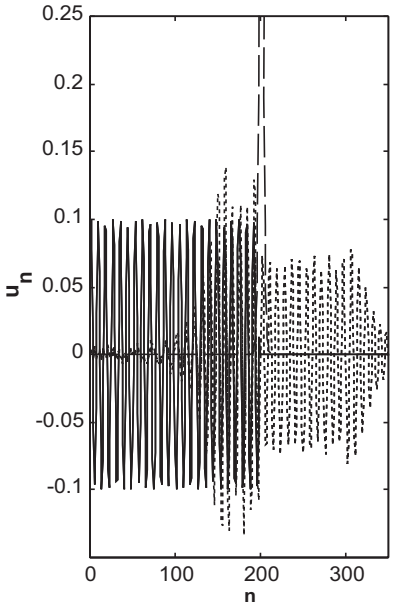

FIG. 9. This figure shows $T=0.62$ for $\gamma=3.5$, $q_b=1.6$, $\lambda=0.5$ for a time period of $t=12$, in agreement with the corresponding theoretical value $T=0.7$ supported by Eq. (43). Different lines in the figure have the same significance as in Fig. 8. Figure clearly shows that a part of the incident wave reflects toward left, which is shown by the dotted line similar to transmitted wave in the right.

On the other hand Fig. 6 presents the T-γ plot for different q_b's while λ is kept constant. PT points of the plot follow as a consequence of Eq. (49) again.

Again since we are considering elastic scattering only, hence, for perfect reflection ($R=1$) we must have $T=0$. On the other hand $T=0$ (for $q_b\neq 0$) implies $\Gamma-H\to\infty$ [see Eq. (43)], which in turn shows that

$$\Gamma = e^{k_a} - e^{-k_a}. \tag{52}$$

As a consequence of that we may have with the aid of Eqs. (13), (45a), and (45c)

$$\gamma\left(1-\frac{1}{2b}\right) = 2(\cos q_b - \lambda - \lambda^{-1} + 1)^{1/2} \times (\cos q_b - \lambda - \lambda^{-1} - 1)^{1/2}, \tag{53}$$

and hence using Eq. (28)

$$\gamma = \lambda - \lambda^{-1} + 4\sqrt{(\cos q_b - \lambda - \lambda^{-1} + 1)(\cos q_b - \lambda - \lambda^{-1} - 1)}. \tag{54}$$

Figure 7 depicts the γ vs λ plot at perfect reflection for different wave vectors q_b on the basis of Eq. (54).

In Figs. 8 and 9 we show the numerical simulation of Eq. (22) using MATLAB in Intel platform. In performing that simulation task we adopt the usual fourth-order Runge-Kutta method on the chain of lattice sites of length $2N+1$ (from $-N$ to N). As the time evolution of the perturbation u_n at each lattice site depends [as suggested by Eq. (22)] on a coupling term involving the value of the perturbation at just the previous and very next lattice sites (namely, u_{n-1} and u_{n+1}), hence, it is quite clear that we cannot define Eq. (22) at the

edges of the lattice, namely, at $n=-N$ and $n=N$. Hence, in our numerical analysis we limit the simulation process of Eq. (22) within the range $n=-N+1$ to $n=N-1$ and take the boundary condition $u_n=0$ at $n=\pm N$.

In fact Fig. 8 shows that a phonon having constant amplitude is incident on the breather solution from the left. After scattering from the breather the transmitted wave travels toward right with the same amplitude as the incident wave, and there is no reflected wave (perfect transmission). On the other hand Fig. 9 reveals that after scattering the transmitted part with diminished amplitude travels toward right and the reflected part also with diminished amplitude travels toward left. All these results confirm our earlier analyses. Both these figures show that the transmitted radiation's amplitude and also the reflected radiation's amplitude in Fig. 9 rapidly diminish near the edges; this happens because of the finite lattice size. The nearest-neighbor linear coupling term in the DNLS equation seems to work well inside the lattice. But as one moves toward the ends of the lattice the coupling gets weaker, and finally just at the end point of the lattice the coupling term does not work at all because of the absence of any further lattice point. This difficulty can be partially removed by taking the lattice size as large as possible, but it will also increase the run time of the simulation program and more errors will be accumulated thereby. We can remove the finite-size error of the lattice in another way by taking a ring [27] instead of the linear lattice. Diminishing of amplitude at the left edge is not so prominent because of the superposition of the reflected and the incident amplitudes. This diminishing in amplitude does not seem to be applicable for incident waves because the incident waves are traveling inward from the left edge, and not toward the edge.

V. CONCLUSION

In this paper we address linear phonon scattering by DBs. Analyses reveal a number of important properties of nonlinear lattices. We have determined exact expressions for T and R in the PWS version of nonlinear model that help us to explore different nonlinear properties.

Discrete breathers are found to be almost transparent for certain specific values of the wave vectors. We have shown that this transparency is to be connected with the existence of breather internal modes. The transmission coefficient changes drastically at a threshold value of the nonlinear parameter when there appears a localized mode about the breather solution. This property is physically relevant to the cases where filtering of some definite frequencies corresponding to maximum energy is required. For example, if a small-amplitude wave packed with phonons with broad time-Fourier spectrum (noise) is sent to the DB, only the phonons with frequencies corresponding to PT are able to pass through the breather.

Again from the condition of PR we observe another feature. We see that there exist certain frequencies for which DBs are almost opaque to the incident phonons. This feature is responsible for a number of nonlinear phenomena, for example, targeted energy transfer, to create large-amplitude breather or to store an amount of breather between DBs, etc., which is important in the context of energy trapping. In the numerical experiment of thermal relaxation in anharmonic systems [28] it was observed that the relaxation rate does not obey the exponential law, but rather it obeys an extended exponential law making the process slower. This phenomenon would become impossible to explain without considering the energy trapping by single DB or between two DBs. In such cases perfect reflection plays a major role. We can also apply the transfer-matrix approach to analyze phonon scattering in another lattice model known as nonlinear discrete Klein-Gordon model (NDKG). In the PWS version of that model we can also show all the results to be exact [17].

ACKNOWLEDGMENT

We acknowledge Professor Tarun K. Roy of Saha Institute of Nuclear Physics, Kolkata for his suggestions regarding the preparation of this manuscript.

[1] A. J. Sievers and S. Takeno, Phys. Rev. Lett. **61**, 970 (1988).
[2] D. K. Campbell, S. Flach, and Y. S. Kivshar, Phys. Today **57**(1), 43 (2004).
[3] S. Aubry, Physica D (Amsterdam) **103**, 201 (1997).
[4] S. Flach and C. R. Willis, Phys. Rep. **295**, 181 (1998).
[5] S. Flach, K. Kladko, and R. S. MacKay, Phys. Rev. Lett. **78**, 1207 (1997).
[6] E. Trias, J. J. Mazo, and T. P. Orlando, Phys. Rev. Lett. **84**, 741 (2000).
[7] P. Binder, D. Abraimov, A. V. Ustinov, S. Flach, and Y. Zolotaryuk, Phys. Rev. Lett. **84**, 745 (2000).
[8] M. Sato *et al.*, Chaos **13**, 702 (2003).
[9] P. W. Anderson, Rev. Mod. Phys. **50**, 191 (1978).
[10] S. F. Helfert, Opt. Quantum Electron. **37**, 185 (2005).
[11] S. Kim, C. Baesens, and R. S. MacKay, Phys. Rev. E **56**, R4955 (1997).
[12] C. Baesens, S. Kim, and R. S. MacKay, Physica D **113**, 242 (1998).
[13] D. Hennig, N. G. Sun, H. Gabriel, and G. P. Tsironis, Phys. Rev. E **52**, 255 (1995).
[14] S. Lee and S. Kim, Int. J. Mod. Phys. B **14**, 1903 (2000).
[15] A. Lahiri, S. Panda, and T. K. Roy, Phys. Rev. Lett. **84**, 3570 (2000).
[16] A. Lahiri, S. Panda, and T. K. Roy, Phys. Rev. E **66**, 056603 (2002).
[17] P. Majumdar and S. Panda (unpublished).
[18] B. I. Swanson, J. A. Brozik, S. P. Love, G. F. Strouse, A. P. Shreve, A. R. Bishop, W. Z. Wang, and M. I. Salkola, Phys. Rev. Lett. **82**, 3288 (1999).
[19] S. Adachi, V. M. Kobryanskii, and T. Kobayashi, Phys. Rev. Lett. **89**, 027401 (2002).
[20] W. P. Su and J. R. Schrieffer, Proc. Natl. Acad. Sci. U.S.A. **77**, 5626 (1980).
[21] G. Kalosakas, S. Aubry, and G. P. Tsironis, Phys. Rev. B **58**,

3094 (1998).
[22] P. G. Kevrekidis, K. O. Rasmussen, and A. R. Bishop, Phys. Rev. E **61**, 4652 (2000).
[23] H. S. Eisenberg, Y. Silberberg, R. Morandotti, A. R. Boyd, and J. S. Aitchison, Phys. Rev. Lett. **81**, 3383 (1998).
[24] R. Morandotti, U. Peschel, J. S. Aitchison, H. S. Eisenberg, and Y. Silberberg, Phys. Rev. Lett. **83**, 2726 (1999).
[25] R. S. MacKay and S. Aubry, Nonlinearity **7**, 1623 (1994).
[26] T. Cretegny, S. Aubry, and S. Flach, Physica D **119**, 73 (1998).
[27] A. Lahiri, P. Majumdar, and A. Lahiri, Phys. Rev. B **72**, 224306 (2005).
[28] R. Reigada, A. Sarmiento, and K. Lidenberg, Chaos **13**, 646 (2003).